Task-Space Control of Articulated Mobile Robots With a Soft Gripper for Operations

doi: 10.1109/TRO.2018.2878361

Task-space Control of Articulated Mobile Robots with a Soft Gripper for Operations

Motoyasu Tanaka, *Member, IEEE,* Kenjiro Tadakuma, *Member, IEEE,* Mizuki Nakajima, and Masahiro Fujita

***Abstract*—A task-space method is presented for the control of a head-raising articulated mobile robot, allowing the trajectory tracking of a tip of a gripper located on the head of the robot in various operations; e.g., picking up an object and rotating a valve. If the robot cannot continue moving because it reaches a joint angle limit, the robot moves away from the joint limit and changes posture by switching the allocation of lifted/grounded wheels. An articulated mobile robot with a gripper that can grasp objects using jamming transition was developed, and experiments were conducted to demonstrate the effectiveness of the proposed controller in operations.**

***Index Terms*—Articulated mobile robot, task-space control, mobile manipulation, redundancy, jamming transition**

I. Introduction

ARTICULATED mobile robots have many segments connected by joints. The segments provide a powered mechanism for propulsion. Such a robot can climb and move around an obstacle, and can propel themselves along narrow paths and change their body posture to follow the terrain. On this basis, many articulated mobile robots have been developed to move inside a pipe [1]–[5], to carry out search and rescue tasks at disaster sites [6]–[13], and to carry out inspection tasks inside nuclear reactors [14], [15].

It is difficult to control an articulated mobile robot because it has many actuators in its joints and propulsion mechanism. A major control method for the articulated mobile robot is shift control [1], [3], [4], [11], [16]–[18]. According to the method, the robot shifts motion from its head to tail. Terrain-following control using torque sensors based on the method have been proposed [17], [18]. Shift control is useful because three-dimensional motion can be generated by simple operation. However, the method is unsuitable for precise positioning of the robot because the motion depends strongly on the operator technique. Another method is called *n-trailer* and uses a model derived assuming that wheels and crawlers do not skid [7], [19]–[21]. If there is no modeling error as wheels skid, a robot can control the position and attitude of its head using the method but the environment is limited to a flat surface. Control methods have been individually proposed for different terrains other than flat terrain; e.g., stairs [8], [12], [22] and the inside and outside of pipes traversed by a snake robot without a propulsion mechanism [23]–[26].

When investigating or inspecting the inside of a building and plant, a robot needs to not only move but also perform operations, such as opening a door and rotating a valve [27], [28]. However, there have been few studies on operations such as grasping and manipulation by articulated mobile robots. The KR-II robot is connected by rotational joints and prismatic joints, with prismatic joints moving in the height direction [15]. A method of controlling the position and attitude of the tip of a gripper on KR-II with a manipulator having few degrees of freedom at the top has been proposed [29], [30]; KR-II realized the mailing of a letter and mobile manipulation using the method. The method allowed the tip of the gripper to be controlled despite the few degrees of freedom of the manipulator by assigning the mechanical degree of freedom of the mechanism for steering to the manipulator. The KR-II robot can also climb stairs and move across rough terrain and can be used for operations in nuclear power plants. KR-II has a small lateral width but is large in the height direction, and can perform works with the mounting of a long arm that accesses high positions.

In contrast, a robot needs to be of low height to enter a narrow space. The ACM-R4 series [16]–[18] and T^2 Snake-3 [22], which are serially connected by rotational joints, can enter such a space because they are of relatively low height. In addition, because the robots can climb a high step by lifting their head along the riser of a step, they perform well in both entering a narrow space and climbing an obstacle. The controlled object in this paper is an articulated mobile robot connected by only rotational joints [16]–[18], [22].

When performing operations such as picking up an object, opening a door, and opening a valve, a robot needs an end effector for gripping and manipulating an object. Mounting a manipulator as a separate mechanism between the end effector and the robot for the grasping and manipulation of objects increases the size of the robot. In contrast, the articulated mobile robot can use part of its body like a manipulator by lifting several links from the end. It is thus possible to reduce the size and mass of a robot using the part normally used for "locomotion" for "operation" as needed [29], [30]. In the case of performing operations by lifting the end of the robot, it is necessary to control the position and attitude of the end portion on which an end effector, such as a gripper, is mounted; i.e., control using the task space.

Many control methods of the position and attitude of the head have been proposed for a snake robot having a similar articulated structure. A snake robot has many links serially

This work was partially supported by the ImPACT Program of Council for Science, Technology and Innovation (Cabinet Office, Government of Japan), and JSPS KAKENHI Grant Number 18K04011.

M. Tanaka and M. Nakajima are with the Department of Mechanical Intelligent Systems Engineering, the University of Electro-Communications, Tokyo 182-8585, Japan. (e-mail: mtanaka@uec.ac.jp).

K. Tadakuma and M. Fujita are with Tohoku University, Sendai 980-8579, Japan.

connected by active joints and all mounted wheels are passive. Models that assume wheels do not skid have been used for control on a flat plane. Control based on kinematics [31], control based on dynamics [32], and control for the application tasks of cooperative transportation [33] and cutting [34] have been proposed. For three-dimensional space, a method of climbing steps by virtually constraining the head on a two-dimensional plane that is parallel to the ground has been proposed [35], [36]. For a flat environment, the three-dimensional trajectory tracking control of the position and attitude of the head has been proposed [37]–[40] with raising of the head but the control cannot be applied to an articulated mobile robot that has active wheels. In the case of the snake robot without wheels, a planning method of raising the head while avoiding falls considering a support polygon [41] has been proposed.

This paper presents a task-space control method for an articulated mobile robot equipped with a gripper at the head, to raise the head and allow the tip of the gripper to track a target trajectory. We use *Omni-gripper* [42], which is an example of a soft gripper, as a compact, lightweight, and multifunctional gripper. A robot having this gripper can grasp an object using not force control but position/velocity control. An articulated mobile robot equipped with an Omni-gripper is developed, and experiments using the proposed control method show that operations involving reaching, grasping, and manipulation, such as picking a small object, turning a valve, and opening a door, can be realized.

The contributions of the paper are as follows.

- The proposed method allows the trajectory tracking of the gripper using not only the raised part of the body but the whole body of the robot. The robot can move forward or backward by behaving like a mobile manipulator [43]. In addition, if the robot cannot continue to move because a joint angle reaches its limit, the proposed method allows the robot to move away from the joint limit by employing redundancy and switching the grounded/lifted wheels.
- An articulated mobile robot equipped with an Omni-gripper is developed, and the robot realizes the operations of picking up a small object, turning a valve, and opening a door.

The remainder of the paper is organized as follows. Section II describes the robot model and the gripper. Section III proposes a task-space control method that allows the controlled point to track a target trajectory. Section IV describes an articulated mobile robot with an Omni-gripper and the customization of the proposed control method to the actual robot. Section V experimentally demonstrates the effectiveness of the proposed control method for operations using the developed robot.

II. Problem Formulation

A. Articulated Mobile Robot

We consider the articulated mobile robot shown in Fig. 1. The robot has a rotational joint around the yaw axis and a rotational joint around the pitch axis, which are connected in series. A pair of wheels are coaxially placed with the pitch joint, and a gripper is attached to the head of the robot. Each wheel is either passive (rotating without actuators) or active

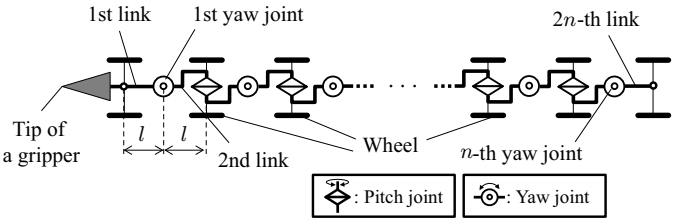

(a) Straight posture

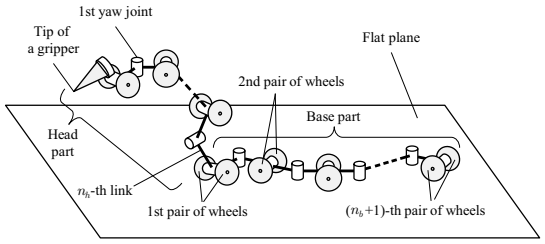

(b) Head raising posture

Fig. 1. Model of an articulated mobile robot.

(rotated by an actuator). Let θ_i be the i-th yaw joint angle and ψ_i be the i-th pitch joint angle. The robot can raise its head using the pitch joints. Figure 1(b) depicts the head raising posture of the robot. Let us define the head part as being constructed from the head to the n_h-th link and the base part as being from the (n_h+1)-th link to the tail end, and we assume that the compositions of the head and base parts do not change. Let $\boldsymbol{\phi}_h = [\theta_1, \psi_1, \cdots, \theta_{\frac{n_h}{2}}, \psi_{\frac{n_h}{2}}]^T \in \mathbb{R}^{n_h \times 1}$ and $\boldsymbol{\phi}_b = [\theta_{\frac{n_h}{2}+1}, \cdots, \theta_n]^T \in \mathbb{R}^{n_b \times 1}$ be the joint angles of the head and base parts, respectively. The number of yaw angles in the base part n_b is $n_b = n - \frac{n_h}{2}$. Let n_w be the total number of active wheels on the base part and ρ_i be the rotation angle of the i-th active wheel on the base part, and we set $\boldsymbol{\rho} = [\rho_1, \cdots, \rho_{n_w}]^T \in \mathbb{R}^{n_w \times 1}$. Active wheels of the head part are ignored.

The environment corresponds to xy plane in the inertial coordinate system $O-xyz$. The robot is teleoperated and the operator provides the steering command while viewing the robot visually or using camera images. The head of the robot is equipped with a gripper, and we let $\boldsymbol{w} = [x_E, y_E, z_E, \alpha_E, \beta_E, \gamma_E]^T$ be the position and attitude of the tip of the gripper, where $\alpha_E, \beta_E, \gamma_E$ are respectively the roll, pitch, and yaw angles in the $O-xyz$ coordinate system. We define $\boldsymbol{\phi} = [\boldsymbol{\phi}_h^T, \boldsymbol{\phi}_b^T]^T$ and $\boldsymbol{q} = [\boldsymbol{w}^T, \boldsymbol{\phi}^T]^T$.

If all the pitch angles of the base part are zero, then all the wheels of the base part are in contact with the ground. If some of the pitch joints slightly rotate, the robot can lift each wheel from the ground [21]. We assume that the motion of pitch joints does not affect the position and attitude of the robot's head and links because we set the desired values of pitch angles of the base part to be small and the dynamic effect of the motion of pitch joints to be weak [21]. We let $\boldsymbol{\psi}_b = [\psi_{\frac{n_h}{2}+1}, \cdots, \psi_{n-1}]^T \in \mathbb{R}^{(n_b-1)\times 1}$ be the pitch angle

of the base part, and assume that they are only used to switch between lifting/grounding of the wheel. From [37], to control six degrees of freedom of the robot's head, the robot has to satisfy the inequality

$$n_h \geq 4. \tag{1}$$

B. Soft Gripper

Soft grippers have a passively deformable part that grasps objects without damaging them. Basically, such grippers have a bag-shaped structure without fingers (e.g., [44]) or fingers with soft joints [45]. From the viewpoint of a lightweight gripper for mobile robots, we chose the former type of gripper without fingers. The structure can grasp an object even if there is some positional error. In general, position and force control is necessary to grasp and manipulate an object. However, if the robot uses a soft gripper, it can grasp and manipulate an object without high-precision position control and force control. We thus use the gripper and aim to realize operations such as reaching, grasping, and manipulation by controlling the position and velocity of the tip of the gripper.

III. Task-space Control

Because an articulated mobile robot has many degrees of freedom, it is difficult and impractical for the operator to directly design the motion of each joint. We thus control the robot in a task space with $\boldsymbol{w}$ as the controlled variable, to change the position and attitude of the gripper $\boldsymbol{w}$.

A. Model

We assume that each wheel does not skid. If all wheels are passive and all wheels of the base part touch the ground, the kinematic model is obtained as [37], [38]

$$\boldsymbol{A}_a(\boldsymbol{q})\dot{\boldsymbol{w}} = \boldsymbol{B}_a(\boldsymbol{q})\dot{\boldsymbol{\phi}}, \tag{2}$$

where $\boldsymbol{A}_a \in \mathbb{R}^{(n_b+4)\times 6}$, $\boldsymbol{B}_a \in \mathbb{R}^{(n_b+4)\times(n_h+n_b)}$, the i-th row ($1 \leq i \leq n_b+1$) is the velocity constraint that the i-th pair of wheels of the base part do not slide sideways, and the j-th row ($n_b+2 \leq j \leq n_b+4$) is the velocity constraint that the base part appropriately makes contact with the ground.

The velocity constraint due to rotation of the active wheel is obtained as [21]

$$\boldsymbol{A}_b(\boldsymbol{q})\dot{\boldsymbol{w}} = \boldsymbol{B}_b(\boldsymbol{q})\boldsymbol{u}, \tag{3}$$

where $\boldsymbol{u} = [\dot{\boldsymbol{\phi}}^T, \dot{\boldsymbol{\rho}}^T]^T$, $\boldsymbol{A}_b \in \mathbb{R}^{n_w\times 6}$, $\boldsymbol{B}_b \in \mathbb{R}^{n_w\times(n_h+n_b+n_w)}$ and the i-th row of the equation is the velocity constraint related to the rotation of the i-th active wheel.

According to (2) and (3), if all wheels of the base part are in contact with the ground, the velocity constraints of the articulated mobile robot are

$$\boldsymbol{A}(\boldsymbol{q})\dot{\boldsymbol{w}} = \boldsymbol{B}(\boldsymbol{q})\boldsymbol{u}, \tag{4}$$

$$\boldsymbol{A} = \begin{bmatrix} \boldsymbol{A}_a \\ \boldsymbol{A}_b \end{bmatrix} \in \mathbb{R}^{(n_b+n_w+4)\times 6}, \tag{5}$$

$$\boldsymbol{B} = \begin{bmatrix} \boldsymbol{B}_a & \boldsymbol{0} \\ & \boldsymbol{B}_b \end{bmatrix} \in \mathbb{R}^{(n_b+n_w+4)\times(n_h+n_b+n_w)}. \tag{6}$$

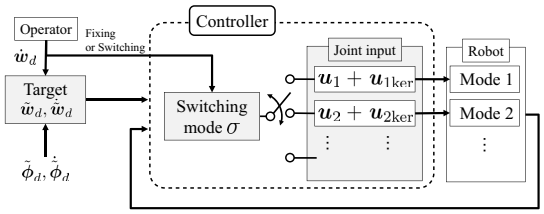

Fig. 2. Task-space control diagram for the articulated mobile robot.

Next, the lifting wheel that does not touch the ground is introduced to the model. Because the model is different depending on the grounded/ungrounded status of each wheel, we allocate a unique integer σ, called the *mode*, to represent the overall status of the wheels. If the $n'_1, \cdots, n'_{\bar{n}_\sigma}$-th pairs of wheels (a total of $\bar{n}_\sigma$ pairs) and $n''_1, \cdots, n''_{\tilde{n}_\sigma}$-th active wheels (a total of $\tilde{n}_\sigma$ active wheels) do not touch the ground in mode σ, the velocity constraints are

$$\boldsymbol{A}_\sigma\dot{\boldsymbol{w}} = \boldsymbol{B}_\sigma\boldsymbol{u}, \tag{7}$$

$$\boldsymbol{A}_\sigma = \begin{bmatrix} \boldsymbol{A}_{a\sigma} \\ \boldsymbol{A}_{b\sigma} \end{bmatrix} \in \mathbb{R}^{(n_b-\bar{n}_\sigma+n_w-\tilde{n}_\sigma+4)\times 6},$$

$$\boldsymbol{B}_\sigma = \begin{bmatrix} \boldsymbol{B}_{a\sigma} & \boldsymbol{0} \\ & \boldsymbol{B}_{b\sigma} \end{bmatrix} \in \mathbb{R}^{(n_b-\bar{n}_\sigma+n_w-\tilde{n}_\sigma+4)\times(n_h+n_b+n_w)}, \tag{8}$$

where $\boldsymbol{A}_{a\sigma} \in \mathbb{R}^{(n_b-\bar{n}_\sigma+4)\times 6}$, $\boldsymbol{B}_{a\sigma} \in \mathbb{R}^{(n_b-\bar{n}_\sigma+4)\times(n_h+n_b)}$, $\boldsymbol{A}_{b\sigma} \in \mathbb{R}^{(n_w-\tilde{n}_\sigma)\times 6)}$, $\boldsymbol{B}_{b\sigma} \in \mathbb{R}^{(n_w-\tilde{n}_\sigma)\times(n_h+n_b+n_w)}$, and $\boldsymbol{A}_{a\sigma}$ and $\boldsymbol{B}_{a\sigma}$ are the matrices whose $n'_1, \cdots, n'_{\bar{n}_\sigma}$-th row vectors are eliminated from the matrices $\boldsymbol{A}_a$ and $\boldsymbol{B}_a$, respectively. $\boldsymbol{A}_{b\sigma}$ and $\boldsymbol{B}_{b\sigma}$ are the matrices whose $n''_1, \cdots, n''_{\tilde{n}_\sigma}$-th row vectors are eliminated from the matrices $\boldsymbol{A}_b$ and $\boldsymbol{B}_b$, respectively. System (7) has kinematic redundancy and the number of redundant degrees of freedom (i.e., the difference between the number of rows and the number of columns of $\boldsymbol{B}_\sigma$) is $n_h+\bar{n}_\sigma+\tilde{n}_\sigma-4$. In this paper, we add shape controllable points (SCPs) to the controlled variable as a representation of a subset of the kinematic redundancy [37]. We introduce the m joint angles $\tilde{\boldsymbol{\phi}} \in \mathbb{R}^{m\times 1}$ into the set of controlled variables, where $\tilde{\boldsymbol{\phi}} = \boldsymbol{S}\boldsymbol{\phi}$ and $\boldsymbol{S} \in \mathbb{R}^{m\times(n_h+n_b)}$ is the selection matrix whose elements are 0 or 1. Let $\tilde{w} = [\boldsymbol{w}^T, \tilde{\boldsymbol{\phi}}^T]^T$ be the controlled variable including the SCP, and ΔT be the switching period for the mode. The kinematic model of the robot with switching modes is represented as

$$\tilde{\boldsymbol{A}}_{\sigma(t)}\dot{\tilde{\boldsymbol{w}}} = \tilde{\boldsymbol{B}}_{\sigma(t)}\boldsymbol{u}, \tag{9}$$
$$\sigma(t) = \sigma(t_k), \quad (t_k \leq t < t_{k+1})$$

where $\sigma \in \{1, 2, \cdots, N_m\}$, N_m is the number of modes, $t_k = k\Delta T$ $(k = 0, 1, \cdots)$ is the switching time of the mode,

$$\tilde{\boldsymbol{A}}_\sigma = \begin{bmatrix} \boldsymbol{A}_\sigma & \boldsymbol{0} \\ \boldsymbol{0} & \boldsymbol{I}_m \end{bmatrix} \in \mathbb{R}^{(n_b-\bar{n}_\sigma+n_w-\tilde{n}_\sigma+4+m)\times(6+m)}, \tag{10}$$

$$\tilde{\boldsymbol{B}}_\sigma = \begin{bmatrix} \boldsymbol{B}_\sigma \\ \boldsymbol{S} \quad \boldsymbol{0} \end{bmatrix} \in \mathbb{R}^{(n_b-\bar{n}_\sigma+n_w-\tilde{n}_\sigma+4+m)\times(n_h+n_b+n_w)}. \tag{11}$$

In (9), the m redundant degrees of freedom are represented as the SCPs, and the remaining redundant degrees of freedom are represented as the null space of $\tilde{\boldsymbol{B}}_\sigma$. This paper uses (9) as the kinematic model of the robot.

B. Joint Input

As shown in Fig. 2, joint input is prepared for each mode, and the robot is controlled by switching the input. Switching the mode σ is also performed by the controller. The operator provides the target of the controlled variable. Details of the switching and the relationship between the operator and controlled variable are explained in the next section.

Controllers with switching modes for a snake robot have been proposed in [46]–[48]. Using a controller, the head of the robot tracks the desired trajectory while various subtasks are performed; e.g., the avoidance of a movable obstacle [46], whole-body collision avoidance [47], and approximate path-tracking for all joints [48]. The controller has been applied for an articulated mobile robot with active wheels in [21]. In such controllers, the kinematic redundancy is represented as null space of the joint input. In [49], we proposed a switching controller where the kinematic redundancy is represented as both the SCPs and null space and realized posture control while maintaining the head position and orientation and avoiding joint limits and self-collision. However, these works deal with only the two-dimensional motion of a robot's head. In this paper, the controller with switching modes is applied for operations of an articulated mobile robot that raises its head. In the controller, the subset of redundancy is represented as the SCP in the head part and is used to reduce the joint load. The remaining degree of redundancy and switching modes are used for joint limit avoidance.

$\boldsymbol{u}$ is designed as

$$\boldsymbol{u} = \boldsymbol{u}_\sigma + \boldsymbol{u}_{\sigma\mathrm{ker}}, \tag{12}$$

$$\boldsymbol{u}_\sigma = \tilde{\boldsymbol{B}}_\sigma^{W\dagger} \tilde{\boldsymbol{A}}_\sigma \left\{ \dot{\tilde{\boldsymbol{w}}}_d - \boldsymbol{K}(\tilde{\boldsymbol{w}} - \tilde{\boldsymbol{w}}_d) \right\}, \tag{13}$$

$$\boldsymbol{u}_{\sigma\mathrm{ker}} = -k_\eta (\boldsymbol{I} - \tilde{\boldsymbol{B}}_\sigma^{W\dagger} \tilde{\boldsymbol{B}}_\sigma) \boldsymbol{\eta}, \tag{14}$$

where $\tilde{\boldsymbol{B}}_\sigma^{W\dagger} = \boldsymbol{W}^{-1} \tilde{\boldsymbol{B}}_\sigma^T (\tilde{\boldsymbol{B}}_\sigma \boldsymbol{W}^{-1} \tilde{\boldsymbol{B}}_\sigma^T)^{-1}$ is a weighted pseudo inverse matrix of $\tilde{\boldsymbol{B}}_\sigma$ [50], $\boldsymbol{W}$ is a positive definite diagonal matrix representing a weight, $\tilde{\boldsymbol{w}}_d$ is a target vector of $\tilde{\boldsymbol{w}}$, $\boldsymbol{K} > \boldsymbol{0}$ is a gain related to the trajectory tracking of the controlled variable, $k_\eta > 0$ is a gain related to the redundancy, and $\boldsymbol{\eta} \in \mathbb{R}^{(n_h+n_b+n_w)\times 1}$ is an arbitrary vector. The elements of $\boldsymbol{u}$ are joint angular velocities and wheel angular velocities. If we use a non-weighted pseudo inverse matrix ($\boldsymbol{W} = \boldsymbol{I}$), the first term on the right side of (12) $\boldsymbol{u}_\sigma$ is the least-squares solution of $|\boldsymbol{u}|$. In this case, the joint velocity is oscillatory because the angular velocity of the wheel becomes dominant at the input norm depending on the condition of the link length and the wheel radius. We therefore use a weighted pseudo inverse matrix so that the joint angular velocity is not oscillatory.

By substituting (12) into (9), the closed-loop system is obtained as

$$\tilde{\boldsymbol{A}}_\sigma \left\{ \dot{\tilde{\boldsymbol{w}}} - \dot{\tilde{\boldsymbol{w}}}_d + \boldsymbol{K}(\tilde{\boldsymbol{w}} - \tilde{\boldsymbol{w}}_d) \right\} = \boldsymbol{0}. \tag{15}$$

If $\tilde{\boldsymbol{A}}_\sigma$ is of full column rank (i.e., if the robot is not a singular configuration), $\tilde{\boldsymbol{w}}$ converges to $\tilde{\boldsymbol{w}}_d$ at $t \to \infty$. So that $\tilde{\boldsymbol{A}}_\sigma$ is of full column rank, the number of rows of $\tilde{\boldsymbol{A}}_\sigma$ has to be no smaller than the number of columns. Thus, the inequality

$$n_b - \bar{n}_\sigma + n_w - \tilde{n}_\sigma \geq 2 \tag{16}$$

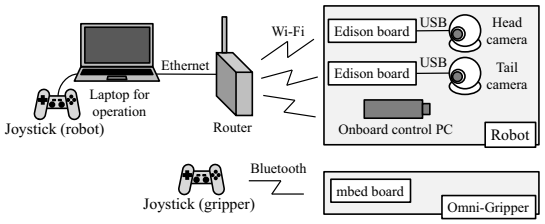

Fig. 3. Experimental system of the robot and gripper.

has to be satisfied from (10).

$\boldsymbol{u}_{\sigma\mathrm{ker}}$ in (12) is a vector depending on the redundancy, and can be used to contribute to achieving sub control objectives (subtasks) without affecting the trajectory tracking of the controlled variable. Let V be the cost function and $\boldsymbol{\eta}$ be designed as

$$\boldsymbol{\eta} = \left[\frac{\partial V}{\partial \varphi_1}, \cdots, \frac{\partial V}{\partial \varphi_{n_h+n_b+n_w}} \right]^T, \tag{17}$$

where $\boldsymbol{\varphi} = [\boldsymbol{\phi}^T, \boldsymbol{\rho}^T]^T \in \mathbb{R}^{(n_h+n_b+n_w)\times 1}$ and φ_i is the i-th element of $\boldsymbol{\varphi}$. The time derivation of V is calculated as

$$\begin{aligned} \frac{\mathrm{d}V}{\mathrm{d}t} &= \frac{\partial V}{\partial \boldsymbol{w}} \dot{\boldsymbol{w}} + \frac{\partial V}{\partial \boldsymbol{\varphi}} \boldsymbol{u} \\ &= \frac{\partial V}{\partial \boldsymbol{w}} \dot{\boldsymbol{w}} + \boldsymbol{\eta}^T \boldsymbol{u}_\sigma - k_\eta \boldsymbol{\eta}^T (\boldsymbol{I} - \tilde{\boldsymbol{B}}_\sigma^{W\dagger} \tilde{\boldsymbol{B}}_\sigma) \boldsymbol{\eta}. \end{aligned} \tag{18}$$

The third term on the right side of (18) contributes to a decrease in V because it is semi-negative definite. It is therefore possible to converge the controlled variable to the target value while achieving the subtask using input (12) and appropriately determining V.

For subsea operations, the underwater swimming manipulator with thrusters has been presented [51]. Although the controlled robots are different, this paper and [51] are similar in terms of the motivation and manipulation methodology used to achieve both the desired motion of the end-effector and secondary tasks (e.g., joint limit avoidance) using kinematic redundancy. Additionally, the control method in [51] has realized the underwater motion of the underwater swimming manipulator by introducing a dynamic controller and thruster allocations. In contrast, the robot in this paper has nonholonomic constraints due to grounded wheels, and the motion of the robot is restricted by the constraints. The control method proposed in this paper can remove the motion restriction by switching modes and allows the robot to move away from the joint limit.

IV. Experimental Setup

Figure 3 depicts the experimental system. An operator uses two joysticks to send the command to the robot and the pump of the gripper.

A. Articulated Mobile Robot

Figure 4 shows the developed articulated mobile robot, which is an improved version of the robot in [22], and Table I

TABLE I
PARAMETERS OF THE T^2 *Snake-3* WITH THE OMNI-GRIPPER.

Number of modules n	9
Link length l [mm]	90.5
Module length L [mm]	181
Total size (H $\times$ W $\times$ L) [mm]	175×175×1729
Wheel radius r [mm]	50
Joint angle range (Pitch) [deg.]	$\lvert\psi_i\rvert \leq 113$
Joint angle range (Yaw) [deg.]	$\lvert\theta_i\rvert \leq 65$
Total mass [kg]	10
Battery life [min.]	about 80

gives the parameters. The performance limits of the robot without the gripper have been demonstrated in [22]. The Omni-gripper and the pump unit for the gripper are respectively equipped at the head and tail of the robot. For a pair of wheels, the wheel on one side is the active wheel and the other wheel is the passive wheel as shown in Fig. 4(b). A ROBOTIS Dynamixel MX-106R and MX-28AR are respectively used for the joint and wheel. Cameras for obtaining images are installed at the head and tail. Batteries are installed for each passive wheel, and the robot can be remotely controlled wirelessly.

The robot in [22] has batteries in the head and tail, but it is necessary to reduce the weights of the head and tail because the head and tail need to carry the gripper and pump, respectively. We thus increase the lengths between the wheels of the first, third, and fifth pairs on the base part as shown in Fig. 4(b), and batteries are relocated from the head and tail to the generated spaces.

In addition, two rotational joints for the gripper are equipped on the head as shown in Figs. 4(e) and 4(f), and the robot can store the gripper as shown in Fig. 4(e) and rotate the gripper as shown in Fig. 4(f) using the joints. By storing the gripper as shown in Fig. 4(e), the robot can climb stairs (Fig. 5(a)) and pass obstacles (Figs. 5(b) and 5(c)) [22].

B. Omni-gripper

Figure 4 shows the Omni-gripper [42], which is an example of a soft gripper. The specifications of the gripper are an outside diameter of 50 mm, length (including the thickness of the cap) of 90 mm, membrane thickness of 7.4 mm, filling amount of powder of 20 g, and weight of 87 g. Thus, even if the gripper is mounted at the head, the robot can lift its head high. The gripper has a powder layer filled with coffee powder. The gripper is usually soft, but by transitioning the powder layer to a vacuum, there is a jamming transition and the gripper hardens. The robot pushes the gripper in a soft state against the object, and the gripper wraps around the object. The gripper can then grasp the object by entering a hardened state as shown in Fig. 4(c). The powder layer is transitioned to a vacuum using the pump unit on the tail as shown in Fig. 4(d).

C. Control Strategy for Actual Experiments

The designed target angle and angular velocity were sent to a Dynamixel actuator. The operator uses a joystick to change the target velocity of the controlled variable $\dot{\boldsymbol{w}}_d$, and $\boldsymbol{w}_d$ is calculated by numerical integration of $\dot{\boldsymbol{w}}_d$. The target value of

(a)

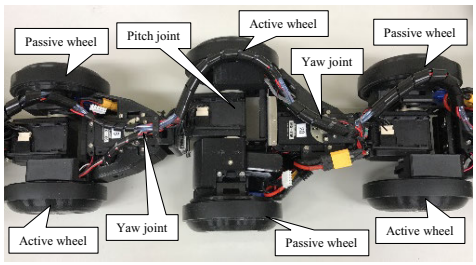

(b)

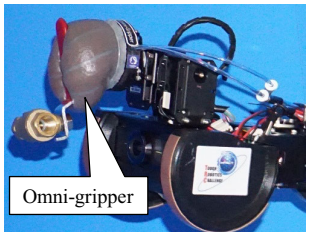

(c)

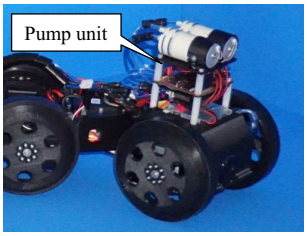

(d)

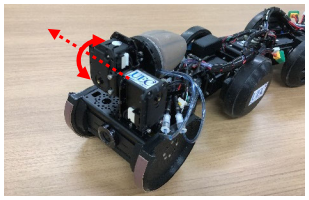

(e)

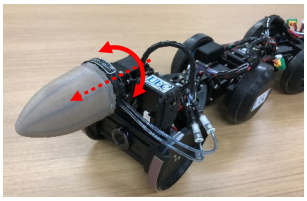

(f)

Fig. 4. Articulated mobile robot T^2 *Snake-3* with the Omni-gripper: (a) whole body, (b) enlarged view of the body, (c) Omni-gripper grasping a valve handle, (d) pump unit for the gripper on the tail, (e) head with a stored gripper, (f) head with a gripper in operation.

the SCP $\tilde{\boldsymbol{\phi}}_d$ is set constant, and we set $\dot{\tilde{\boldsymbol{\phi}}}_d = \boldsymbol{0}$. The onboard control personal computer receives the joint angle of the robot, calculates the joint input velocity using (12), and sends the target angle and target angular velocity for each actuator.

1) Estimation of the Controlled Variable: In an environment without an external measuring device, the estimated

(a) (b) (c)

Fig. 5. Motion examples of T^2 *Snake-3* with the Omni-gripper: (a) semiautonomous stair climbing, (b) climbing a desk, (c) climbing two pipes arranged vertically.

position and attitude of the controlled point are calculated using the joint angle of the head part because the head position and attitude cannot be measured. In this case, assuming that the base part makes proper contact with the plane, z_E, α_E, and β_E can be calculated. x_E and y_E are calculated by integrating the target velocity.

2) Feedforward Control: The robot has a large load on the pitch joint when it lifts its head and a steady error occurs for the pitch joint angle of the head part because the servo stiffness of the actuator is not sufficient with respect to the magnitude of the load. If a steady error occurs for the pitch joint angle of the head part, a steady error also occurs for the estimated position and attitude of the controlled point z_E, α_E, β_E, which are calculated using the joint of the head part. When control is performed using the current joint angle information of the robot, control commands are given to the wheels and the joints so as to compensate for the steady error occurring for the position and attitude of the controlled point. The error of the pitch joint of the head part under high load is a steady error and the angle does not follow the target value forever, but the wheel continues to rotate. As a result, even when the operator's command is not given, minute translational movement due to rotation of the wheels continued and made the robot difficult to steer. We thus control the robot by perfect feedforward control based on the target angular velocity given by the operator. The joint angle of the robot is estimated by integrating the target angular velocity, and the actual joint angle of the robot is not used at all in the calculation of the joint input. The joint input $\boldsymbol{u}$ is calculated by substituting the estimated value of the controlled variable and $\dot{\boldsymbol{w}}_d$ into (12). The target velocity and the target angle calculated using the numerical integral are then output to the robot. Because the servo stiffness of the joint of the base part is sufficient, the angle almost matches the target value. In contrast, although there are steady errors in the joint angle of the head part, there is no difficulty in steering because the wheels stop rotating when the operator's command is not given.

3) Shape Controllable Point: A large load is applied to the n_h-th joint because it is a joint between the head part and base part. We thus let the n_h-th joint be the SCP and define $\tilde{\phi} = \psi_{\frac{n_h}{2}}$, and allow the robot to directly control the n_h-th joint. The target value of $\psi_{\frac{n_h}{2}}$, which is an element of the controlled variable, is designed by considering the load torque of the n_h-th joint. By reducing the distance on the xy plane between the head of the robot and the n_h-th joint, the load torque can be kept small. In experiments, we set $n_h = 6$ and the target value $\psi_{\frac{n_h}{2}d}$ of the $\psi_{\frac{n_h}{2}}$ is set to 110 degrees, which is the neighborhood of the joint angle limit as shown in Fig. 4(a).

4) Cost Function: It is more difficult for an articulated mobile robot with active wheels to enter a singular configuration than a snake robot for which all wheels are passive [52]. We do not consider the singularity avoidance because the robot in the paper has many active wheels and it was experimentally confirmed that the robot does not enter a singular configuration.

The limit angle of the yaw joint of the developed robot is 65 degrees. Then, if the base part of the robot moves backward, the yaw joint frequently reaches the angle limit and the robot cannot continue operation. We thus design the cost function V as

$$V = \boldsymbol{\phi}^T \boldsymbol{K}_V \boldsymbol{\phi}, \tag{19}$$

where $\boldsymbol{K}_V \geq \boldsymbol{0}$ is a diagonal matrix. The robot reduces each joint angle by decreasing the value in (19), and accomplishes joint limit avoidance.

5) Mode Switching: By switching modes, the allocation of grounded/ungrounded wheels is changed and the space of redundancy changes with the mode. The robot can select the mode considering the effect on the cost function. Thus, the articulated mobile robot effectively accomplishes both trajectory tracking and the subtask (e.g., avoiding a movable obstacle [21]). In contrast, when the robot raises its head as in this paper, mode switching has detrimental effects, such as introducing vibration and position error to the head motion. In this paper, the robot has two states related to the switching of modes. One is the fixing state while the other is the switching state. In the fixing state, the robot fixes the mode and does not switch mode to suppress the head error. The robot is usually in the fixing state and can change state under the command of the operator as shown in Fig.2. The switching state is used when the joint of the robot reaches the angle limit and the robot does not continue to move, and mode switching is then performed and the joint angle is reduced until the robot becomes operable.

In [21], the robot selects the optimal mode for the subtask when switching mode but the calculation cost is high. In the present paper, the robot heuristically changes mode according to a prescripted order to reduce the calculation cost. We use the mode numbers as in Table II and set the mode number of the fixing state as $\sigma = 1$. In the switching state, mode numbers 2 to 6 are used and mode switching is repeated as $\sigma = 2, 3, \cdots, 6, 2, 3, \cdots$. The robot attempts a straight posture in order from the tail to the head of the base part, and it is expected that the robot will recover from the state where the joint angle reaches the limit.

The robot has the following features related to lifted wheels.

- The more adjacent the lifted wheels are, the larger the motion of the lifted part is during joint limit avoidance.
- The more lifted wheels there are, the more readily the robot falls as a result of a lack of grounded wheels.

TABLE II
MODE AND WHEEL STATUS

Mode num. σ	Wheel num. (L: lifted, G: grounded)						
	1	2	3	4	5	6	7
1	G	G	L	G	G	L	G
2	G	G	G	G	G	L	L
3	G	G	G	G	L	L	G
4	G	G	G	L	L	G	G
5	G	G	L	L	G	G	G
6	G	L	L	G	G	G	G

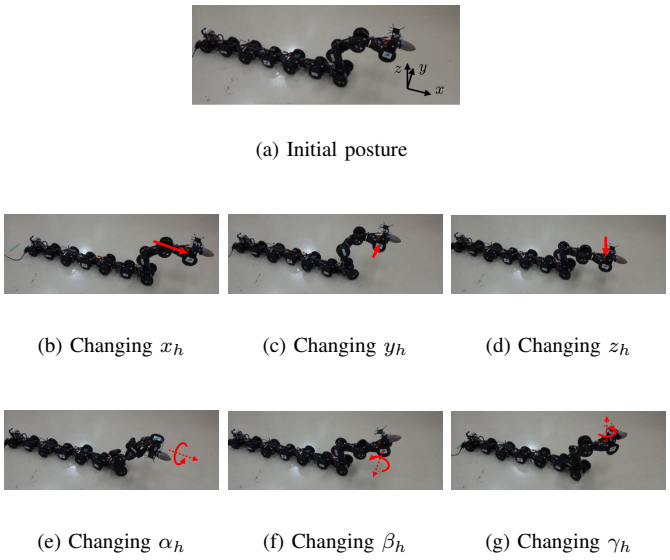

(a) Initial posture

(b) Changing x_h (c) Changing y_h (d) Changing z_h

(e) Changing α_h (f) Changing β_h (g) Changing γ_h

Fig. 6. Initial and terminal postures in experiments on relative position accuracy.

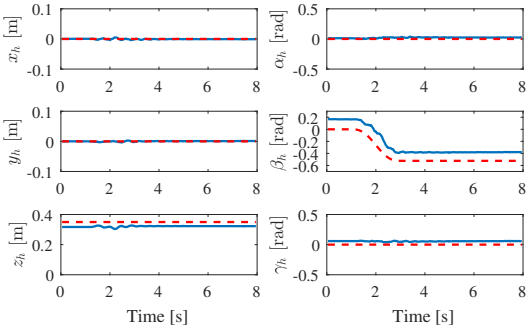

(a) Using the estimated value of $\boldsymbol{w}_h$.

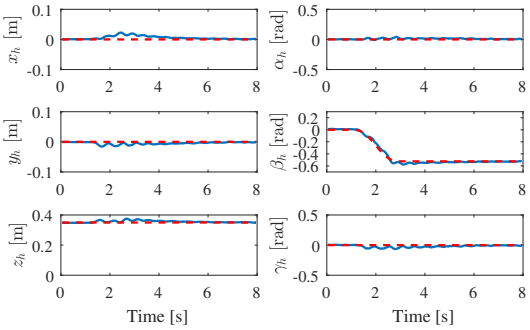

(b) Using $\boldsymbol{w}_h$ measured by the motion capture system.

Fig. 7. $\boldsymbol{w}_h$ in the case of changing β_h. The red dotted line is the target value while the blue line is the actual measurement.

- If there is no lifted wheel, the robot does not have kinematic redundancy.
- The robot cannot simultaneously lift three adjacent wheels and the wheel of the head of the base part because of a lack of torque.

We thus select modes 2–6 in which only two wheels are lifted as shown in Table II.

6) Number of Lifted Links: n_h must satisfy (1). If the robot lifts many links and uses them as the head part, the range of motion of the head part increases. Thus, if there is no upper limit of joint torque, it is better to lift as many links as possible. However, if there are few links in the base part, the robot readily falls. In this way, there is a trade-off relationship between the number of links of the head part and the static stability.

We set $n_h = 6$ because it is the maximum number depending on the maximum joint torque. It then seems that the robot does not readily fall because the base part has twice as many links as the head part.

V. EXPERIMENT

A. Relative Position Accuracy

The position accuracy of the proposed control method was verified. Because the gripper is flexible, its tip position varies depending on its weight and the condition of the internal powder. An experiment was thus performed by modifying the model and the control input with the position and attitude of the robot's head $\boldsymbol{w}_h = [x_h, y_h, z_h, \alpha_h, \beta_h, \gamma_h]^T$ as the controlled point instead of the tip of the gripper. The initial posture of the base part was straight and we set $\boldsymbol{\phi} = [0, -0.8, 0, -1.1, 0, 1.9, 0, \cdots, 0]^T$ as the initial values of the joint angles. Each element of the target value of $\boldsymbol{w}_h$ was independently varied. The position and attitude of the head were measured with a motion capture system (OptiTrack, NaturalPoint, Inc.). The initial and terminal postures are shown in Fig. 6, and an example of the result obtained when changing β_h is shown in Fig. 7(a).

There was steady error in z_h and β_h as shown in Fig. 7(a). It seems that this error is due to the heaviness of the head part and insufficient servo stiffness and mechanical stiffness.

We calculate the terminal value of $\boldsymbol{w}_h$ by averaging $\boldsymbol{w}_h$ at $t_e + 4 \leq t \leq t_e + 5$, where $t = t_e$ is the time at which the change in the target value of $\boldsymbol{w}_h$ is complete. The target value begins to change at $t = 1$ and we also calculate the initial value by averaging $\boldsymbol{w}_h$ at $0 \leq t \leq 1$. Let $\Delta\boldsymbol{w}_h = [\Delta x_h, \Delta y_h, \Delta z_h, \Delta\alpha_h, \Delta\beta_h, \Delta\gamma_h]^T$ be the relative displacement between the initial value and terminal value of $\boldsymbol{w}_h$. Experiments were performed five times for each motion, and the relative displacement of the position and

TABLE III
EXPERIMENTAL RESULTS OF RELATIVE DISPLACEMENT

	Δx_h [m]	Δy_h [m]	Δz_h [m]	$\Delta\alpha_h$ [rad]	$\Delta\beta_h$ [rad]	$\Delta\gamma_h$ [rad]
Target value	0.20	0	0	0	0	0
Exp. (Mean)	0.20	0.0052	0.0024	0.0092	-0.0047	-0.012
Exp. (SD)	0.0025	0.0015	0.00082	0.0061	0.015	0.0059
Error	1.0%	–	–	–	–	–
Target value	0	0.1	0	0	0	0
Exp. (Mean)	-0.069	0.066	0.014	-0.055	-0.055	-0.075
Exp. (SD)	0.0036	0.0033	0.00071	0.0053	0.0047	0.0039
Error	–	34%	–	–	–	–
Target value	0	0	-0.1	0	0	0
Exp. (Mean)	-0.011	0.0040	-0.10	0.013	-0.013	0.0075
Exp. (SD)	0.0017	0.00081	0.00090	0.0042	0.0050	0.0033
Error	–	–	1.5%	–	–	–
Target value	0	0	0	π/2	0	0
Exp. (Mean)	-0.054	-0.035	0.030	1.54	-0.060	-0.063
Exp. (SD)	0.0042	0.0018	0.0011	0.014	0.0051	0.0037
Error	–	–	–	1.9%	–	–
Target value	0	0	0	0	-π/6	0
Exp. (Mean)	0.00062	0.0015	0.0061	0.019	-0.55	-0.0060
Exp. (SD)	0.0013	0.0011	0.00094	0.0061	0.0063	0.0047
Error	–	–	–	–	6.0%	–
Target value	0	0	0	0	0	π/4
Exp. (Mean)	-0.018	0.00032	0.027	0.050	-0.12	0.79
Exp. (SD)	0.0020	0.0016	0.00057	0.0073	0.0070	0.0084
Error	–	–	–	–	–	0.4%

attitude was compared with the target relative displacement. Table III gives the results. The error was calculated using the target relative displacement and the average value of the relative displacement in five experiments. The errors in Δx_h, Δy_h, Δz_h, $\Delta\alpha_h$, $\Delta\beta_h$, and $\Delta\gamma_h$ were 1.0, 34, 1.5, 1.9, 6.0, and 0.4%, respectively.

The error in the motion that changes y_h was large while the errors in the other motions were small. We consider the error in the motion that changes y_h. In the motion, it was observed that the active wheel at the head of the base part slipped during operation. As a result, it seems that the error occurred because the head moved not only in the y direction but also in the $-x$ direction.

Although the model of the control method is derived assuming that the wheels do not skid, the wheels do indeed slip and there is error for the controlled point. If the robot is remotely controlled, the operator needs to compensate for the error by operating a joystick.

Fig. 7(b) shows the result obtained using not the estimate value but $\boldsymbol{w}_h$ measured by the motion capture system when calculating the joint input (12) in the case of changing β_h. It was confirmed that $\boldsymbol{w}_h$ converged to the desired value when using the actual value of the controlled variable, even if there was modeling error, such as that relating to the skidding of wheels and insufficient stiffness of the motor. If the position and orientation can be measured or estimated with high accuracy (e.g., employing simultaneous localization and mapping), the controlled variable converges to the target value as given by (15).

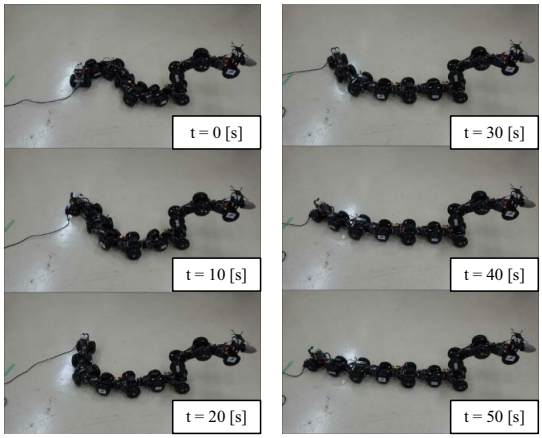

Fig. 8. Motion of the robot in the case of switching σ.

B. Joint Limit Avoidance

When the base part has a zigzag form and the joint angles of the base part reach their limit at $t = 0$ in Fig. 8, the robot can hardly move the controlled point. The robot thus needs to return to a posture that allows it to better move the controlled point. Experiments on joint limit avoidance were performed using mode switching described in section IV-C5. We set $\Delta t = 1$, fixed the mode at $t < 2$ (i.e., the fixing state), switched the mode at $t \geq 2$ (i.e., the switching state), and set the diagonal elements of $\boldsymbol{K}_V$ as $(15,\ 0.015,\ 15,\ 0.015,\ 15,\ 0.015,\ 9.6,\ 4.8,\ 2.4,\ 1.2,\ 0.6,\ 0.3)$. In $\boldsymbol{K}_V$, the element corresponding to the yaw angle in the head part is larger than that of the pitch angle because the angle range of the yaw joint is smaller than that of the pitch joint. We designed $\boldsymbol{K}_V$ such that the element corresponding to the base part doubled in value in order from the tail to the head of the base part, to prioritize the joint limit avoidance for the angle of the forward joint.

Figures 9 and 10 show the results. The cost function decreased V with time. Although the angle of the base part $\theta_4, \cdots, \theta_9$ was in the neighborhood of the joint angle limit (1.1 rad), the angle decreased with time. It is seen that the posture of the robot improved in order from the tail to the head by mode switching. Figure 9 shows that the position error and attitude error were about 30 mm and 0.1 rad, respectively.

As mentioned above, although there was some error in the position and attitude of the controlled point, it was confirmed that the joint limit was avoided and the robot returned from an inoperative posture.

C. Contact Force

The contact force of the robot's head was measured. Figure 11 shows the measurement system. We used a PFS055YA251U6 (Leptrino Co. Ltd) force sensor. The robot pushed the plate and the force sensor measured the contact force. We measured the maximum contact forces f_x, f_y, f_z along x, y, $-z$ directions five times each by controlling the position of the head. In experiments, the posture of the robot was straight or L-shaped. Tables IV and V give the results obtained by setting the posture as shown in Fig. 12(a) and 12(b), respectively.

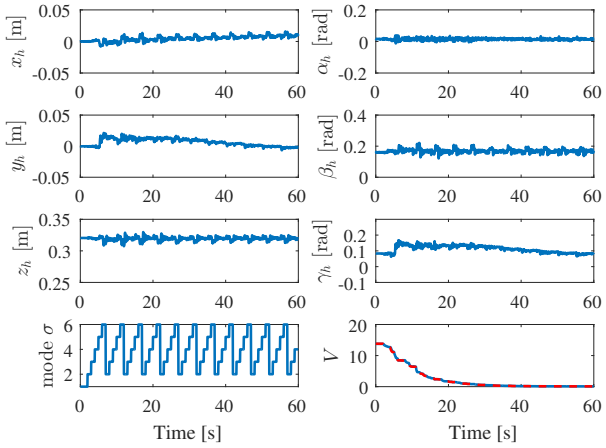

Fig. 9. $\boldsymbol{w}_h$, σ, and V in the case switching σ. In the graph of V, the red dotted line is calculated from the target value while the blue line is calculated from the actual measurement of the robot.

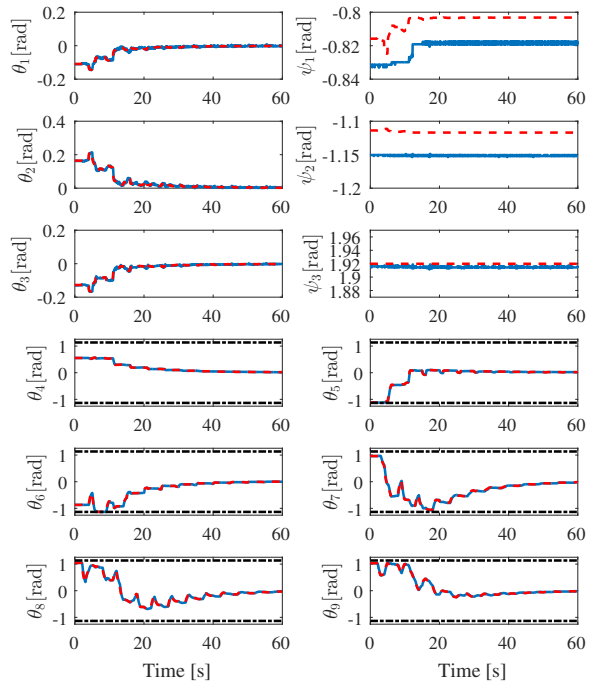

Fig. 10. $\boldsymbol{\phi}$ in the case switching σ. The red dotted line is the target value while the blue line is the actual measurement, and the black dot-and-dash line is the joint angle limit.

The results show that the force is strong in the case of the initial posture where the force exerted by wheels of the base part is efficiently transmitted to the head. If the posture is straight and z_h is small as for posture (iii), f_x is largest. In contrast, f_x is small when z_h is large, y_h is large, or the direction of the contact force does not correspond to the direction of the wheels on the base part. These results show that the base part has a strong effect on the contact force. Thus,

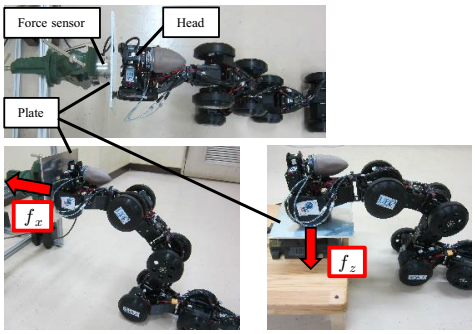

Fig. 11. Measurement system of the contact force.

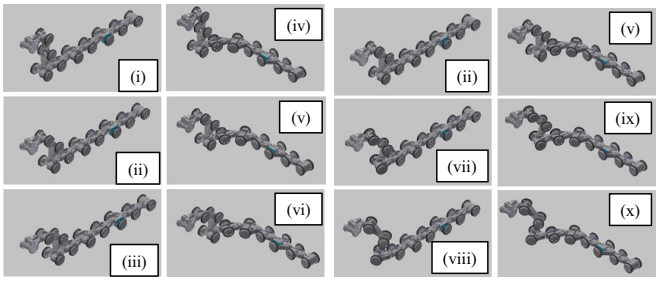

(a) Changing z_h (b) Changing y_h

Fig. 12. Initial posture of the robot in the case of measuring contact force.

if the robot has to generate a strong contact force, the robot should change posture such that the force exerted by wheels is efficiently transmitted to the contact point.

The propulsion force exerted by the wheels of the base part does not affect f_z. In fact, even when changing the posture of the base part, f_z is almost the same. Thus, similar to the case for the manipulator, if the robot changes posture as the head part efficiently generates f_z, the robot can generate large f_z.

D. Application Experiments

Using the proposed control method and the developed robot with the gripper, operations requiring reaching, grasping, and manipulation were carried out as application experiments. The operator issued commands to the robot and gripper by joystick while viewing the robot visually. The controlled point of the control input was the tip of the gripper.

1) Picking Up an Object: The robot requires reaching and grasping functionalities to pick up an object on the ground. The robot pushed the gripper in a soft state against the object while reaching for the object, and the gripper then hardened and grasped the object. The robot was able to pick up a T-joint pipe on the ground as shown in Fig. 13.

2) Rotating a Valve: Reaching, grasping, and manipulation are required to rotate a valve. Video [53] showing the robot rotating a gate valve. The robot first pushed the gripper in a soft state against the valve so that the center of the gripper aligned with the center of the valve. The gripper grasped the handle of the valve by hardening, and the robot rotated the

TABLE IV
CONTACT FORCES ($y_h = 0$, CHANGING z_h)

			f_x[N]	f_y[N]	f_z[N]
Posture	z_h[m]	Base part	Mean±SD	Mean±SD	Mean±SD
(i)	0.40	Straight	16.9±0.3	5.71±0.22	15.7±0.3
(ii)	0.35	Straight	24.0±1.1	8.60±0.20	12.1±0.1
(iii)	0.30	Straight	30.4±1.7	9.72±0.33	10.1±0.2
(iv)	0.40	L-shape	14.9±0.3	5.41±0.36	15.5±0.2
(v)	0.35	L-shape	21.4±0.5	7.1±0.5	11.3±0.2
(vi)	0.30	L-shape	26.3±1.1	9.94±0.35	10.3±0.2

TABLE V
CONTACT FORCES ($z_h = 0.35$, CHANGING y_h)

			f_x[N]	f_y[N]	f_z[N]
Posture	y_h [m]	Base part	Mean±SD	Mean±SD	Mean±SD
(ii)	0.0	Straight	24.0±1.1	8.60±0.20	12.1±0.1
(vii)	0.1	Straight	20.4±0.4	11.1±0.5	13.2±0.2
(viii)	0.2	Straight	15.0±0.5	10.1±0.9	15.5±0.3
(v)	0.0	L-shape	21.4±0.5	7.12±0.48	11.3±0.2
(ix)	0.1	L-shape	19.2±1.1	12.7±0.6	13.5±0.4
(x)	0.2	L-shape	13.5±0.5	14.9±1.1	16.1±0.2

valve by rotating the joint located at the base of the gripper. In this way, the operator completed the task without sending a complex command to the robot.

3) Opening a Door with a Knob: Figure 14 shows the robot opening a door on which a small knob is attached. In this case, mobile manipulation is needed after the robot grasps the knob. The robot grasped the knob, and the robot succeeded in opening the door under the operator's appropriate command. The operator provided a command for the yaw angle of the controlled point so that the gripper was always perpendicular to the door. Figure 14(d) and (f) shows that the joint reached the limit angle and the robot could not move backward. However, the robot changed posture as shown in Fig. 14(e) and (g) while maintaining the position and attitude of the controlled point employing mode switching, and the robot was able to resume moving backward.

E. Discussion

When an articulated mobile robot lifts its head, there is likely error in the head positioning because the head part is a cantilever structure. In contrast, the Omni-gripper is robust against positioning error. The robot and gripper have a complementary relationship in that one complements the other's defect; this is an integrated example with good compatibility.

In the case of rotating a valve reported in the present study, although there was a mismatch between the rotational axis of the handle of the valve and the rotational axis of the joint attached on the base of the gripper, the task was completed through only rotation of the joint attached on the base of the gripper after the gripper grasped the handle. This is because the position error and deflection, which are caused by the low stiffness of the position control of the servo motor of the joint on the head part, were large. This indicates that the robot adapts passively by deflection of the joint to some extent even if there is error in the axis of rotation of the motion.

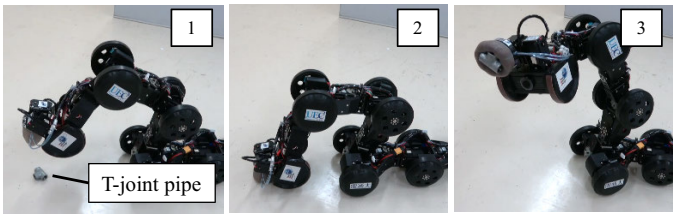

Fig. 13. Picking up a T-joint pipe. 1: Reaching, 2: Grasping, 3: After picking up.

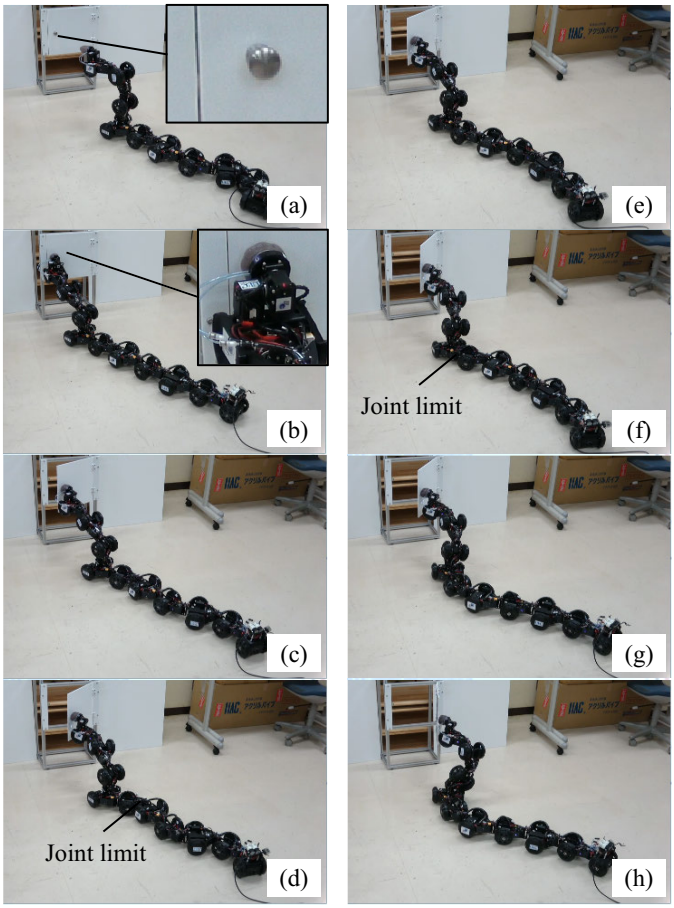

Fig. 14. Opening a door with a knob: (a) initial posture, (b) the gripper grasping the handle, (c) and (h) opening the door, (d) and (f) joint reaching its limit, (e) and (g) after the switching of modes for joint limit avoidance.

In contrast, when the gripper makes contact with an object, there is positioning error of the gripper in the positive direction of the z axis because the deflection of the robot is eliminated. The operator then needs to provide a command to correct the position.

The robot cannot rotate a valve with a diameter that cannot be wrapped with the gripper because the gripper cannot grasp such a valve. Additionally, it is impossible to rotate a valve that requires torque exceeding the maximum gripping torque of the gripper.

Using the cost function (19), the base part adopts a straight configuration as in Fig. 8. The straight configuration is weak in terms of resisting a torque applied around the longitudinal

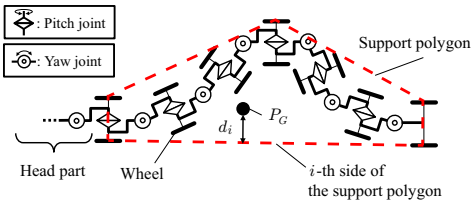

Fig. 15. Support polygon and P_G of the robot (top view).

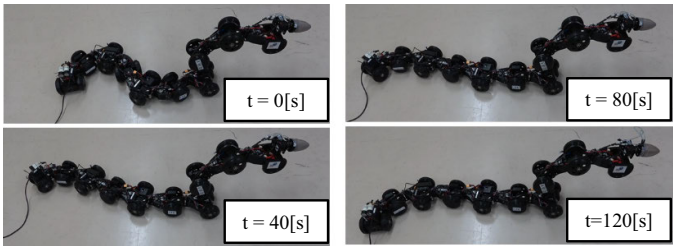

Fig. 16. Motion of the robot obtained using the modified cost function (20).

axis of the body. However, the robot hardly falls because the load is concentrated on the base part and the body posture is often extended in an effort to avoid joint limits, and the present paper does not consider fall avoidance. The falling of the robot can be prevented by considering the support polygon [41], [54] and introducing the distance between the center of gravity and the support polygon into the cost function. The robot is statically stable when the projective point P_G of the robot's center of gravity in the environment is contained within the support polygon of the grounded wheels. For example, we set the cost function V as

$$V = a_1 \boldsymbol{\phi}^T \boldsymbol{K}_V \boldsymbol{\phi} + a_2 \frac{1}{||\boldsymbol{d}||_2}, \tag{20}$$

where $a_1 > 0$ and $a_2 > 0$ are weight constants, $\boldsymbol{d} = [d_1, d_2, \cdots]$ and d_i is the distance from P_G to the i-th side of the support polygon. Figure 15 shows the support polygon and d_i. Figure 16 shows the experimental results obtained using the modified cost function (20), where the initial posture is the same as that in Fig. 8. In this case, the robot did not adopt a straight posture and the area of the support polygon was greater than that in the case of Fig. 8. Note that the support polygon changes greatly depending on the mode switching. It is thus better that the robot uses not heuristic mode switching as used in this paper but switching optimized by predictive calculation as in [21].

If the robot exerts a strong force on the object in an operation, it is necessary to introduce the zero-moment point considering not only the center of gravity but also the reaction force of the object. The optimal posture of the robot in terms of avoiding falls thus depends on the reaction force. It is future work to design the optimal posture for maximizing the contact force while avoiding falls.

Although the operator conducted experiments while observing the robot and the surroundings visually, it is necessary to operate the robot in a real environment using only the camera image. It is a future task to add a camera to obtain images suitable for operations.

VI. Conclusion

This paper proposed a task-space control method for an articulated mobile robot equipped with a gripper at the head of the robot. When the robot cannot continue moving because the joint angle reaches its limit, the method allows the robot to move away from the joint limit using redundancy and by switching modes. An articulated mobile robot with the Omni-gripper was developed, and experiments on joint limit avoidance and for verification of the positioning accuracy were carried out. In addition, picking up an object, opening a valve, and opening a small door with a knob were accomplished as applications.

In future work, we aim to use the developed robot for plant patrol inspection as a practical use, improve the mobility and operational performance, and improve the hardware durability of the robot.

References

[1] B. Klaassen, K. L. Paap, "GMD-SNAKE2: A Snake-Like Robot Driven by Wheels and a Method for Motion Control," *Proc. IEEE Int. Conf. on Robotics and Automation*, pp.3014-3019, 1999.

[2] K. -U. Scholl, V. Kepplin, K. Berns, and R. Dillmann, "Controlling a Multijoint Robot for Autonomous Sewer Inspection," *Prc. IEEE Int. Conf. on Robotics and Automation*, pp.1701-1706, 2000.

[3] H. Streich and O. Adria, "Software Approach for the Autonomous Inspection Robot MAKRO," *Proc. IEEE Int. Conf. on Robotics and Automatin*, pp.3411-3416, 2004.

[4] A. A. Fjerdingen, P. Liljebäck, and A. A. Transeth, "A snake-like robot for internal inspection of complex pipe structures (PIKo)," *Proc. IEEE/RSJ Int. Conf. on Intelligent Robots and Systems*, pp.5665-5671, 2009.

[5] A. Kakogawa and S. Ma, "Design of a Multilink-articulated Wheeled Inspection Robot for Winding Pipelines: AIRO-II," *Proc. IEEE/RSJ Int. Conf. on Intelligent Robots and Systems*, pp.2115-2121, 2016.

[6] K. Osuka and H. Kitajima, "Development of mobile inspection robot for rescue activities: MOIRA," *Proc. IEEE/RSJ Int. Conf. on Intelligent Robots and Systems*, pp. 3373-3377, 2003.

[7] T. Kamegawa, T. Yamasaki, H. Igarashi, and F. Matsuno, "Development of the Snake-like Rescue Robot 'KOHGA'," *Proc. IEEE Int. Conf. on Robotics and Automation*, pp.5081-5086, 2004.

[8] J. Borenstein, M. Hansen, and A. Borrell, "The OmniTread OT-4 Serpentine Robot – Design and Performance," *J. of Field Robotics*, vol.24, no.7, pp.601-621, 2007.

[9] M. Arai, Y. Tanaka, S. Hirose, H. Kuwahara, and S. Tsukui, "Development of "Souryu-IV" and "Souryu-V:" Serially connected crawler vehicles for in-rubble searching operations," *J. of Field Robotics*, vol.25, issue 1, pp.31-65, 2008.

[10] K. Suzuki, A. Nakano, G. Endo, and S. Hirose, "Development of Multi-wheeled Snake-like Rescue Robots with Active Elastic Trunk," *IEEE/RSJ Int. Conf. on Intelligent Robots and Systems*, pp.4602-4607, 2012.

[11] H. Komura, H. Yamada, S. Hirose, G. Endo, and K. Suzumori, "Development of snake-like robot ACM-R8 with large and mono-tread wheel," *Advanced Robotics*, vol.29, no.17, pp.1081-1094, 2015.

[12] K. Ito and H. Maruyama, "Semi-autonomous serially connected multi-crawler robot for search and rescue," *Advanced Robotics*, vol.30, no.7, pp.489-503, 2016.

[13] L. Pfotzer, S. Klemm, A. Roennau, J. M. Zöllner, and R. Dillmann, "Autonomous Navigation for Reconfigurable Snake-Like Robots in Challenging, Unknown Environments," *Robotics and Autonomous Systems*, 2016. (DOI: 10.1016/j.robot.2016.11.010)

[14] S. Hirose and A. Morishima, "Design and Control of a Mobile Robot with an Articulated Body," *The Int. J. of Robotics Research*, vol.9, no.2, pp.99-114, 1990.

[15] S. Hirose, A. Morishima, and S. Tsukagosi, "Design of Practical Snake Vehicle: Articulated Body Mobile Robot KR-II," *Proc. Fifth Int. Conf. on Advanced Robotics*, pp.833-838, 1991.
[16] H. Yamada and S. Hirose, "Development of Practical 3-Dimensional Active Cord Mechanism ACM-R4," *J. of Robotics and Mechatronics*, vol.18, no.3, pp.305-311, 2006.
[17] H. Yamada, S. Takaoka, and S. Hirose, "A snake-like robot for real-world inspection applications (the design and control of a practical active cord mechanism)," *Advanced Robotics*, vol.27, no.1, pp.47-60, 2013.
[18] K. Kouno, H. Yamada, and S. Hirose, "Development of Active-Joint Active-Wheel High Traversability Snake-Like Robot ACM-R4.2," *J. of Robotics and Mechatronics*, vol.25, no.3, pp.559-566, 2013.
[19] H. Fukushima, S. Satomura, T. Kawai, M. Tanaka, T. Kamegawa, and F. Matsuno, "Modeling and Control of a Snake-like Robot Using the Screw Drive Mechanism," *IEEE Trans. on Robotics*, vol.28, no.3, pp.541-554, 2012.
[20] B. Murugendran, A. A. Transeth and S. A. Fjerdingen, "Modeling and path-following for a snake robot with active wheels," *IEEE/RSJ Int. Conf. on Intelligent Robots and Systems*, pp. 3643-3650, 2009.
[21] M. Tanaka, M. Nakajima, and K. Tanaka, "Smooth Control of an Articulated Mobile Robot with Switching Constraints," *Advanced Robotics*, vol.30, no.1, pp.29-40, 2016.
[22] M. Tanaka, M. Nakajima, Y. Suzuki, and K. Tanaka, "Development and Control of Articulated Mobile Robot for Climbing Steep Stairs," *IEEE/ASME Trans. on Mechatronics*, vol.23, issue 2, pp.531-541, 2018.
[23] D. Rollinson and H. Choset, "Pipe Network Locomotion with a Snake Robot," *J. of Field Robotics*, vol.33, issue 3, pp.322-336, 2016.
[24] T. Kamegawa, T. Baba, and A. Gofuku, "V-shift control for snake robot moving the inside of a pipe with helical rolling motion," *Proc. 2011 IEEE Int. Symp. on Safety, Security and Rescue Robotics*, pp.1-6, 2011.
[25] T. Takemori, M. Tanaka, and F. Matsuno, "Gait Design of a Snake Robot by Connecting Simple Shapes," *Proc. 2016 IEEE Int. Symp. on Safety, Security and Rescue Robotics*, pp.189-194, 2016.
[26] M. Vespignani, K. Melo, M. Mutlu, and A. J. Ijspeert, "Compliant snake robot locomotion on horizontal pipes," *Proc. IEEE Int. Symp. Safety, Security Rescue Robotics*, 2015.
[27] J. Pellenz, A. Jacoff, T. Kimura, E. Mihankhah, R. Sheh, and J. Suthakorn, "RoboCup Rescue Robot League," In *RoboCup 2014: Robot World Cup XVIII*, pp.673-685, 2014.
[28] G. Pratt and J. Manzo, "The DARPA Robotics Challenge [competitions]," *IEEE Robotics & Automation Magazine*, vol.20, no.2, pp.10-12, 2013.
[29] E. F. Fukushima, S. Hirose, and T. Hayashi, "Basic Manipulation Consideration For The Articulated Body Mobile Robot," *Proc. IEEE/RSJ Int. Conf. on Intelligent Robots and Systems*, pp.386-393, 1998.
[30] E. F. Fukushima and S. Hirose, "Integration of Locomotion and Manipulation Control for Articulated Body Mobile Robots," *J. of Robotics Society of Japan*, vol.18, no.8, pp.1112-1121, 2000 (in Japanese).
[31] F. Matsuno and K. Mogi, "Redundancy Controllable System and Control of Snake Robot with Redundancy based on Kinematic Model", *Proc. IEEE Int. Conf. on Decision and Control*, pp. 4791-4796, 2000.
[32] F. Matsuno and H. Sato, "Trajectory Tracking Control of Snake Robots based on Dynamic Model," *Proc. IEEE Int. Conf. on Robotics and Automation*, pp.3029-3034, 2005.
[33] M. Tanaka and F. Matsuno, "Cooperative Control of Two Snake Robots," *Proc. IEEE Int. Conf. on Robotics and Automation*, pp.400-405, 2006.
[34] S. Nansai, M. R. Elara, and M. Iwase, "Dynamic Hybrid Position Force Control using Virtual Internal Model to realize a cutting task by a snake-like robot," *6th IEEE Int. Conf. on Biomedical Robotics and Biomechatronics*, pp.151-156, 2016.
[35] M. Tanaka and K. Tanaka, "Control of a Snake Robot for Ascending and Descending Steps," *IEEE Trans. on Robotics*, vol.31, no.2, pp.511-520, 2015.
[36] K. Kon, M. Tanaka, and K. Tanaka, "Mixed Integer Programming Based Semi-autonomous Step Climbing of a Snake Robot Considering Sensing Strategy," *IEEE Trans. on Control Systems Technology*, vol.24, no.1, pp.252-264, 2016.
[37] M. Tanaka and F. Matsuno, "Modeling and Control of Head Raising Snake Robots by Using Kinematic Redundancy," *J. of Intelligent & Robotic Systems*, vol.75, no.1, pp.53-69, 2014.
[38] F. Matsuno and K. Suenaga, "Control of Redundant 3D Snake Robot Based on Kinematic Model," *Proc. IEEE Int. Conf. on Robotics and Automation*, pp.2061-2066, 2003.
[39] M. Yamakita, M. Hashimoto, and T. Yamada, "Control of Locomotion and Head Configuration of 3D Snake Robot (SMA)," *Proc. IEEE Int. Conf. on Robotics and Automation*, pp.2055-2060, 2003.
[40] S. Ma, Y Ohmameuda, K. Inoue, and B. Li, "Control of a 3-Dimensional Snake-like Robot," *Proc. IEEE Int. Conf. on Robotics and Automation*, pp.2067-2072, 2003.
[41] E. A. Cappo and H. Choset, "Planning End Effector Trajectories for a Serially Linked, Floating-base Robot with Changing Support Polygon," *American Control Conference*, pp.4038-4043, 2014.
[42] M. Fujita, K. Tadakuma, H. Komatsu, E. Takane, A. Nomura, T. Ichimura, M. Konyo, and S. Tadokoro, "Jamming Layered Membrane Gripper Mechanism for Grasping Differently Shaped-Objects Without Excessive Pushing Force for Search and Rescue," *Advanced Robotics*, accepted.
[43] O. Khatib, "Mobile manipulation: The robotic assistant," *Robotics and Autonomous Systems*, vol.26, issues 2-3, pp.175-183, 1999.
[44] G. Bancon and B. Huber, "Depression and Grippers with Their Possible Applications," *Proc. 12th Int. Symp. on Industrial Robots*, pp.321-329, Paris, 1982.
[45] S. Hirose and Y. Umetani, "The development of soft gripper for the versatile robot hand," *Mechanism and machine theory*, vol.13, no.3, pp.351-359, 1978.
[46] M. Tanaka and F. Matsuno, "Control of Snake Robots with Switching Constraints: trajectory tracking with moving obstacle," *Advanced Robotics*, vol.28, issue 6, pp.415-429, 2014.
[47] M. Tanaka, K. Kon, and K. Tanaka, "Range-sensor-based Semiautonomous Whole-body Collision Avoidance of a Snake Robot," *IEEE Trans. on Control Systems Technology*, vol.23, no.5, pp.1927-1934, 2015.
[48] M. Tanaka, K. Tanaka, and F. Matsuno, "Approximate Path-Tracking Control of Snake Robot Joints with Switching Constraints," *IEEE/ASME Trans. on Mechatronics*, vol.20, no.4, pp.1633-1641, 2015.
[49] M. Tanaka and K. Tanaka, "Shape Control of a Snake Robot With Joint Limit and Self-Collision Avoidance," *IEEE Trans. on Control Systems Technology*, vol.25, no.4, pp.1441-1448, 2017.
[50] D. P. Martin, J. Baillieul, and J. M. Hollerbach, "Resolution of Kinematic Redundancy Using Optimization Techniques," *IEEE Trans. on Robotics and Automation*, vol.5, no.4, pp.529-533, 1989.
[51] J. Sverdrup-Thygeson, E. Kelasidi, K. Y. Pettersen, and J. T. Gravdahl, "The Underwater Swimming Manipulator–A Bioinspired Solution for Subsea Operations," *IEEE J. of Oceanic Engineering*, DOI: 10.1109/JOE.2017.2768108. (early access article)
[52] M. Tanaka and K. Tanaka, "Singularity Analysis of a Snake Robot and an Articulated Mobile Robot with Unconstrained Links," *IEEE Trans. on Control Systems Technology*, vol.24, no.6, pp.2070-2081, 2016.
[53] https://www.youtube.com/watch?v=3uI7YB3zY4o&t=334s (2018. 4. 9)
[54] S. Toyoshima, M. Tanaka, and F. Matsuno, "A Study on Sinus-Lifting Motion of a Snake Robot with Sequential Optimization of a Hybrid System," *IEEE Trans. on Automation Science and Engineering*, vol.11, no.1, pp.139-144, 2014.

Motoyasu Tanaka (S'05 - M'12) received his B.Eng., M.Eng., and Ph.D. degrees in Engineering from the Department of Mechanical Engineering and Intelligent Systems at the University of Electro-Communications, Japan in 2005, 2007, and 2009, respectively. From 2009 to 2012, he worked at Canon, Inc., Tokyo, Japan. He is currently an Associate Professor in the Department of Mechanical and Intelligent Systems Engineering at the University of Electro-Communications. His research interests include biologically inspired robotics and dynamics-based nonlinear control. He received the IEEE Robotics and Automation Society Japan Chapter Young Award from the IEEE Robotics and Automation Society Japan Chapter in 2006, and the Best Poster Award at SWARM2015: The First International Symposium on Swarm Behavior and Bio-Inspired Robotics in 2015.

Kenjiro Tadakuma (S'04 - M'07) received his Ph.D degree in mechanical and aerospace engineering from the Tokyo Institute of Technology in 2007. He is currently an associate professor of the Graduate School of Information Sciences, Tohoku University. His research interests mainly include mechanisms, omnidirectional mobile robots and rescue robots. He is the recipients of the Young Scientist's Prize for the Commendation of Science and Technology by the Minister of Education, Culture, Sports, Science and Technology (MEXT) in 2011. He is a member of the IEEE, RSJ, JSME, SICE, JSDE, JSRM.

Mizuki Nakajima received his B.Eng. and M.Eng. degrees in Engineering from the Department of Mechanical Engineering and Intelligent Systems at the University of Electro-Communications, Tokyo, Japan in 2014, and 2016, respectively. He is currently a Ph. D. candidate in the Department of Mechanical and Intelligent Systems Engineering at the University of Electro-Communications. His research interests include the development and control of snake robots.

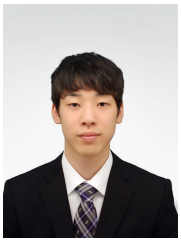

Masahiro Fujita received his B. Eng. from the Kobe City College of Technology, Japan in 2016. He is currently a Master's student at the Human-Robot Informatics Laboratory in Information and Applied Technology, Tohoku University. His current research interests are development of soft-robotic gripper based on Jamming transition.